Journal of The
Electrochemical Society

Galvanic Corrosion between Mild Steel and Iron Sulfides in Acidic Solutions: Part I. Experimental Factors

To cite this article: Payman Sharifi Abdar *et al* 2025 *J. Electrochem. Soc.* **172** 011501

Journal of The Electrochemical Society, 2025 **172** 011501

Galvanic Corrosion between Mild Steel and Iron Sulfides in Acidic Solutions: Part I. Experimental Factors

Payman Sharifi Abdar,[z] **Bruce Brown, and Srdjan Nesic**

Institute for Corrosion and Multiphase Technology, Department of Chemical and Biomolecular Engineering, Ohio University, Athens, 45701 Ohio, United States of America

With the increase in production of sour oil and gas fields, mitigation of production-related failures due to H_2S corrosion of mild steel is a key challenge. In H_2S environments, most failures occur due to localized corrosion originating from the galvanic coupling between mild steel and conductive iron sulfide corrosion products. However, the mechanism of the galvanic coupling between mild steel and iron sulfides and the effect of influential parameters, have not been studied yet. Here, we provide a systematic experimental investigation on the galvanic corrosion between mild steel and iron sulfides by examining the effect of the critical factors: iron sulfide type, cathode to anode surface area ratio, and salt concentration. Specifically, we focus on pyrite and pyrrhotite as the main corrosion products found in localized corrosion of mild steel in H_2S environments. Our results show that the cathodic current obtained on pyrrhotite was an order of magnitude higher than that obtained on pyrite, leading to a higher galvanic current for coupled mild steel-pyrrhotite compared to coupled mild steel-pyrite. Moreover, our study reveals that the increase of cathode to anode surface area ratio and, to some extent, the increase of salt concentration, enhance the galvanic current for the coupled materials.

 [DOI: 10.1149/1945-7111/ada2ba]

Manuscript submitted September 7, 2024; revised manuscript received December 11, 2024. Published January 2, 2025.

Supplementary material for this article is available online

H_2S corrosion, also known as "sour" corrosion, is one of the well-researched types of mild steel degradation related to oil and gas transmission pipelines. This is because localized corrosion is known to be the main type of corrosion failure in sour environments which caused 12% of all oilfield corrosion incidents according to a report from 1996.[1] That being the case, control and mitigation procedures for this type of corrosion could prevent such failures in oil and gas industries, and significantly enhance asset integrity while reducing maintenance costs as well as eliminating environmental damages.

The unpredictability of localized corrosion in sour media is a complicated challenge as several factors, such as the nature of the corrosion products and the contribution of galvanic coupling, play a role in this type of corrosion.[2–4] Iron sulfides, as the corrosion products in H_2S corrosion of mild steel, consist of various polymorphs (i.e., mackinawite, pyrite, pyrrhotite) with different physicochemical and electrical properties. The physicochemical and thermodynamic properties of iron sulfides have been investigated previously.[5–7] Although the formation of these iron sulfides was shown to somewhat protect the surface of mild steel from uniform corrosion by forming a diffusion barrier, their conductive nature was directly associated with the presence of localized attacks.[4,8–12]

The corrosive effect of various polymorphs of iron sulfides on mild steel has been reported for decades.[13,14] Although galvanic coupling between iron sulfides and mild steel has been thought for a long time to be the main mechanism leading to localized corrosion on mild steel in H_2S environments, the experimental verification of this mechanism has been recently examined.[15–17] In one of the first studies done in this area, Ning et al.[15] showed that galvanic coupling between pyrite and mild steel could cause severe localized corrosion, by designing a set of experiments to separate the influence of galvanic coupling from the chemical effects on the localized corrosion of mild steel in H_2S environments. In these experiments, the presence of pyrite particles on API 5L X65 steel surface in 1 wt. % NaCl solution at pH 4, 25 °C, and 0.1 bar pH_2S for one week, resulted in severe localized attacks on the surface of mild steel. In order to investigate the chemical effects, a thin nylon mesh with a 60 μm pore size was placed between pyrite particles and mild steel surface in the exact same experimental conditions, and no localized attack was observed. This study revealed that the localized corrosion of mild steel in presence of iron sulfides has an electrochemical nature, and thus proposed the galvanic coupling as the mechanism of these localized attacks.[15] However, the proposed mechanism is just the first step for achieving the final goal, which is the prediction of localized corrosion of mild steel in aqueous H_2S solutions. Prior to developing a prediction model, experimental data for the galvanic corrosion of mild steel in presence of different iron sulfides as well as for the surface chemistry of iron sulfides are required.

So far, only few studies, which were reported as conference papers, have measured galvanic corrosion between iron sulfides and mild steel in order to examine the proposed galvanic mechanism and understand the effect of experimental parameters on it.[16–19] In one of the previous studies, Tjelta et al.[16] experimented the electrochemical behavior of iron sulfides including pyrite, pyrrhotite and troilite in various pH values in aqueous H_2S solutions. In addition, the galvanic current and potential were measured when these iron sulfides were coupled to API 5L X65 steel. The results revealed that all iron sulfides act as cathodes when coupled to mild steel, however, pyrite showed the largest ability to polarize the surface of mild steel while pyrrhotite-steel couple produced the highest galvanic current. The result seemed somewhat contradictory as the material that polarizes the mild steel most is expected to produce the highest galvanic current. The authors discussed that the source of this discrepancy could emerge from the semiconductive characteristic of pyrite leading to higher polarization of mild steel.[16] Tjelta et al. also tested the galvanic coupling between mackinawite and mild steel and found that mackinawite causes small galvanic effect when the sizes of cathode and anode are equal.[20] In another research, Yepez et al.[17] studied the galvanic coupling between carbon steel C1018 and two iron sulfide samples: pyrite, and mixture of pyrrhotite and troilite. It was shown that corrosion current of mild steel increased due to coupling to both samples when mixture of pyrrhotite and troilite sample produced slightly higher current.[17] Finally, in 2018 Navabzadeh[19] investigated the galvanic coupling between API 5L X65 steel and two iron sulfides: pyrite, and pyrrhotite in various environment at pH 4. The results showed that steel-pyrrhotite couple generates slightly higher galvanic current compared with steel-pyrite couple in N_2, CO_2, and H_2S sparged solutions. However, a significant decline of galvanic current was

[z]E-mail: ps782416@ohio.edu

observed during all measurements which was associated with surface reduction in case of pyrrhotite and hydrogen permeation in case of pyrite. Furthermore, the surface area of iron sulfide cathodes were not clearly determined in this study.[19]

Although these studies confirmed that the corrosion rate of mild steel significantly increased due to the galvanic coupling with iron sulfides, they lacked a systematic investigation of the effect of various influential experimental parameters such as cathode to anode surface area ratio, pH, etc. Apart from the discrepancies that were mentioned above, the experimental designs of these studies are subjected to one major drawback: the surface areas of the electrodes were not properly defined. One of the decisive factors in galvanic coupling phenomena is the ratio of cathode to anode surface area. Specifically in the case of localized corrosion of mild steel in H_2S environments, the porosity of iron sulfides, in some cases, results in a very high surface area of cathode which intensifies the rate of cathodic current. Therefore, interpreting the results of galvanic measurements while ignoring the surface area of electrodes is not conclusive, and in some cases, could even be misleading.

After reviewing the literature dedicated to galvanic coupling measurements, it would be beneficial to concisely review another body of literature covering studies which investigated the under-deposit corrosion of mild steel in presence of iron sulfides. In these cases, the localized attack occurring in under-deposit corrosion also stems from the galvanic coupling between the surface of mild steel and the deposited particles. Thus, these studies might provide more insights into the underlying mechanism. Unfortunately, the studies in this area are also very limited. For instance, Kvarekval et al.[21] studied the effect of FeS (mixture of pyrrhotite and troilite) deposits on the surface of UNS K03014 carbon steel in H_2S/CO_2 environments. The results showed that the presence of FeS deposits significantly increased the weight loss corrosion and created severe localized attacks. The localized penetration depth increased 20 times in some cases. The same experiments were performed in presence of sand deposits, and the results indicted a very low rate of localized corrosion.[21] Ning et al.[4,22] investigated the corrosion of API 5L X65 mild steel under pyrite and sand deposits in H_2S and CO_2 environments. Severe localized corrosion was observed in presence of pyrite while no localized attack was observed in presence of sand particles. In addition, the effect of the size of pyrite particles on localized corrosion was examined and it was concluded that the smaller particles lead to deeper localized pits. The authors stated that smaller particles provides larger cathodic surface area.[22] This observation is evidence for the importance of cathode to anode surface area ratio. Lastly, the influence of the presence of pyrrhotite layer on mild steel surface in various NaCl concentrations in CO_2 and mixed H_2S/CO_2 environments was investigated by Navabzadeh et al.[8,19] A significant observation was that the localized corrosion rate in 1 wt.% NaCl solutions was reported three times higher than the solution without NaCl. This result not only showed that the presence of a pyrrhotite layer enhances localized corrosion of mild steel, but also substantiated the galvanic nature of localized attack due to its change with solution conductivity. In conclusion, all the under-deposit studies mentioned here reaffirmed that the corrosion rate of mild steel is increased when coupled to iron sulfides.

Following the gap analysis above, in the present work we aim to extend the mechanistic understanding of localized corrosion of mild steel in sour environments due to galvanic coupling between the mild steel and iron sulfides. Herein, in the first part of our study, we investigate the effect of influential experimental parameters: type of iron sulfide, cathode to anode surface area ratio, and salt concentration, on the galvanic corrosion of mild steel due to coupling to iron sulfides. Understanding the impact of these factors should lead to revealing the proper mechanism of galvanic corrosion of mild steel in sour environments. We selected pyrite and pyrrhotite as these corrosion products have been mostly found when localized attack of mild steel was observed in presence of H_2S, according to previous studies.[4,9,10] Cathode to anode surface area ratio is another important factor in this process as the high porosity of iron sulfides formed on the surface of mild steel could increase the surface area of iron sulfides (cathode) to one or two order of magnitudes higher than the mild steel (anode). This high ratio could significantly amplify the effect of galvanic coupling and intensify the localized attack. For this reason, we designed a specific experimental setup in this study such that the surface area of electrodes are clearly determined. We also examined the effect of salt concentration as another influential factor since higher salt concentration increases galvanic current by facilitating the electrical current transfer in solution. It is worth noting that all the experiments have been performed in acidic solutions without the presence of dissolved H_2S. This was done for the sake of simplicity in this stage of research, in order to clearly understand the importance of influential factors listed above.

Materials and Methods

Materials.—We designed a specific experimental setup for this study in order to fulfill the objectives of galvanic coupling measurements and avoid the discrepancies observed in previous studies. API 5L X65 was selected to make a mild steel specimen with the composition shown in Table I, and pyrite and pyrrhotite were selected to make iron sulfides specimens. Mineral pyrite and pyrrhotite were purchased from Ward's Science. For purity analysis, these rock-like minerals were powdered by pestle and mortar, then characterized by XRD measurement using Cu Kα radiation as shown in Fig. 1. Very high purity was observed for pyrite sample when compared to the reference pattern ICDD# 00-0042-1340.[23] For pyrrhotite sample, comparing the XRD data to the reference pattern ICSD# 01-079-5969[24] confirms that sample is mainly composed of monoclinic crystal structure. In addition, the composition of the pyrrhotite sample was calculated based on (1 0 2) peak of XRD data, as shown in the supplementary materials, and it was found to have the formulae of $Fe_{0.92}S$. Small peaks that do not match the reference pattern might originate from the fact that natural mineral pyrrhotite is generally composed of various crystal structures, i.e., hexagonal, with different non-stoichiometry compositions which show slightly different XRD peaks.[25] To ensure the purity of pyrrhotite specimen, Raman spectroscopy was performed at the surface of polished pyrrhotite electrode using a Bruker confocal Raman microscope SENTERRA II, and the result (Fig. S1) fits very well with the reference spectra of pyrrhotite.[26,27] A more in-depth analysis of the purity of pyrrhotite sample is provided in the supplementary materials.

Experimental design.—As mentioned, we carefully manufactured the exposed surface areas of the test specimen in order to obtain the desired cathode to anode surface area ratios. The cathode to anode surface area ratio varied from 1:1, and to the exact values of 8.2:1 and eventually 91.1:1. The goal was to change the area ratio by

Table I. Chemical composition of API 5L X65 carbon steel (in wt.%).

Cr	Cu	Mn	Mo	C	Co	Ni	Si	Ti	As
0.25	0.17	1.51	0.09	0.05	<0.001	0.29	0.17	0.01	0.008
P	S	Al	Sn	Sb	V	Zr	Nb	Fe	
0.004	<0.001	0.028	0.002	<0.001	0.04	<0.001	0.03	balance	

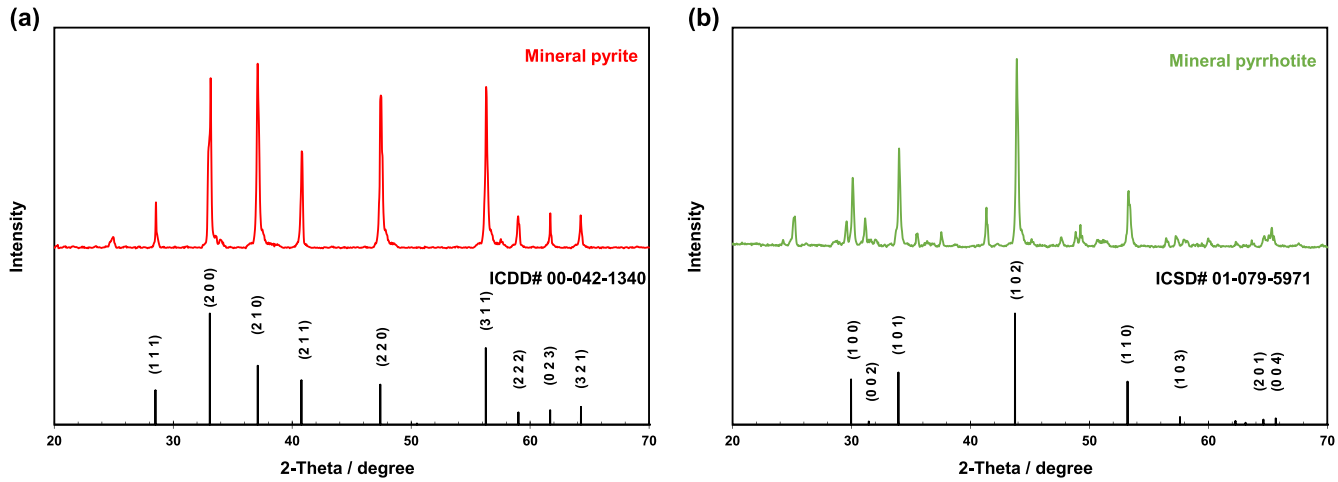

Figure 1. XRD analysis of mineral iron sulfide samples. (a) pyrite, (b) pyrrhotite.

one and then two orders of magnitude in order to detect the noticeable impact of this factor. In this study, in order to simplify the illustrations, the ratios will be rounded off and reported as 1:1, 8:1, and 90:1. The actual size of specimens was selected based on manufacturing limitations. The API 5L X65 steel and mineral iron sulfides specimens with two different surface areas, 0.196 and 0.0177 cm^2 for mild steel and 0.196 and 1.613 cm^2 for iron sulfides, were cut to the desired shape. The back of each of the iron sulfide minerals were attached to a wire using silver conductive paste and the whole assembly was embodied in epoxy leaving only the front surface area exposed. The X65 steel samples were soldered to a wire and also completely embodied in epoxy leaving only the front surface area exposed. These two electrodes were placed on a designed stainless-steel holder with a fixed distance of two centimeters separating them, as shown in Fig. 2. The two electrodes were insulated from each other while connected externally through a zero-resistance ammeter (ZRA). A platinum-coated titanium mesh counter electrode was placed in the middle between these two electrodes. Also, a Luggin capillary connected to an Ag/AgCl (sat. KCl) reference electrode (RE) was kept between the platinum counter electrode (CE) and the working electrode (WE). The electrodes were facing each other in this design so that the current distribution would be uniform. The experiments were performed in an unstirred condition to eliminate the effect of flow. The whole electrochemical setup was placed in a 2-liter glass cell at 30 °C and 1 bar atmospheric pressure as seen in Fig. 2 (refer to Fig. S2 for the actual images of specimens) for all the experimental measurements.

Electrochemical measurements.—Prior to each experiment, the 2-litter glass cell was filled with NaCl solution and de-aerated with nitrogen for at least half an hour. A stir bar was used during this time to achieve a uniformly mixed and deoxygenated solution, and then the solution pH was set to the desired value. All electrodes were polished with 400 and 600 grit abrasive papers, then washed with isopropyl alcohol and finally dried with N_2 gas. For the galvanic coupling measurements, the mild steel electrode was immersed and coupled to the iron sulfide electrode for 2 h during which galvanic current and galvanic potential were measured using the zero-resistance ammeter (ZRA) method. The 2-hour test duration was chosen so that the measurements reach stability, but also to avoid significant formation of corrosion product layers on the surface of mild steel. In order to observe the behavior of mild steel electrode during galvanic measurements, the open circuit potential (OCP) and the corrosion rate of uncoupled steel were measured, using linear polarization resistance (LPR) method. For this purpose, we uncoupled the mild steel electrode from iron sulfide electrode every 30 min, performed the OCP and LPR measurements on the steel

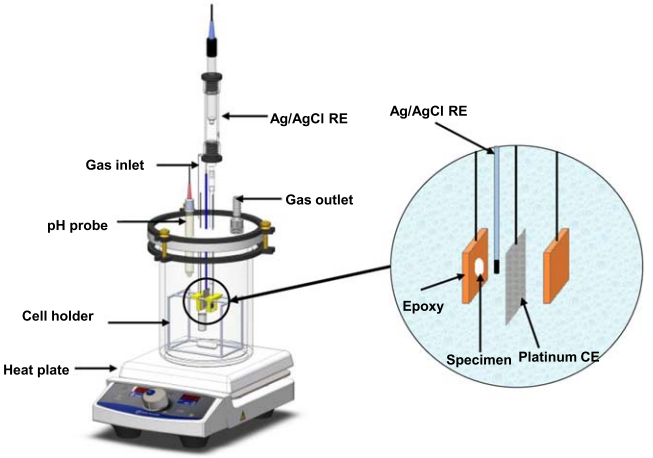

Figure 2. Illustration of the experimental design and the arrangement of electrochemical cell.

specimen, then re-coupled the two and resumed with the galvanic current and potential measurements. At the end of the two-hour long galvanic experiment, potentiodynamic polarization sweeps with the scan rate of 0.5 $mV \cdot s^{-1}$ were performed on both electrodes. Prior to each experiment, solution resistance was also measured by performing electrochemical impedance spectroscopy (EIS) experiment at OCP in the frequency range of 10000–1 Hz with a peak-to-peak AC voltage amplitude of 10 mV. The solution resistance data were then used to correct the potentials for LPR, ZRA, and potentiodynamic measurements. All electrochemical measurements were performed using a Gamry potentiostat Reference 600.

The solution was kept at pH 5.0 for most experiments, using HCl and NaOH, in order to mimic the pH in field conditions, and the pH drift during the galvanic measurements was less than 0.1 which therefore showed minimal impact on the results. However, we did change the pH in a few experiments, which will be described in the last section of the paper.

The effect of aqueous solution conductivity was investigated using three different salt concentrations. We changed the initial concentration of 1 wt.% NaCl in water, by an order of magnitude, down to 0.1 wt.% and up to 10 wt.% NaCl.

In summary, using the experimental design and procedures described above (see Table SI for the complete test matrix), we were able to examine the effect of three key experimental parameters on galvanic corrosion of mild steel when coupled with iron sulfide in

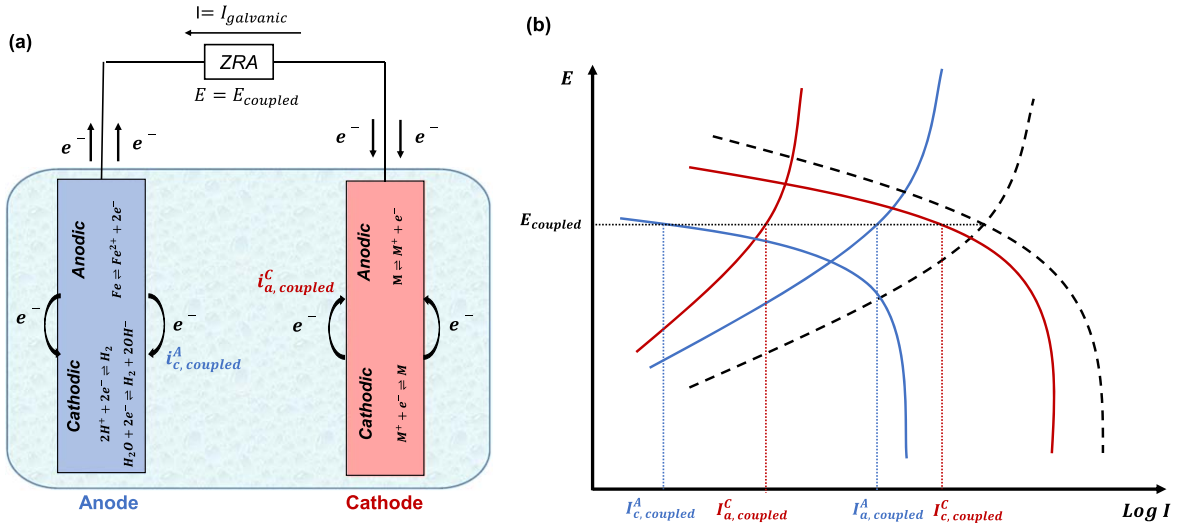

Figure 3. (a) Schema of coupled mild steel-iron sulfide system including the relevant electrochemical reactions. (b) A qualitative example of polarization curves of anode (blue lines), cathode (red lines), and their associated galvanic couple (black lines) for a general galvanic couple cell.

aqueous solutions: iron sulfide type, cathode to anode surface area ratio, and solution conductivity.

Results and Discussion

The system of galvanic coupling between mild steel and iron sulfides can be schematized as Fig. 3a. When the materials are coupled during the ZRA measurement, anodic and cathodic reactions occur at the surface of both electrodes. In the case of mild steel electrode, previous studies revealed that, in mildly acidic solutions, iron dissolution (Reaction 1) occurs as the anodic reaction and hydrogen evolution due to hydrogen ions (Reaction 2) as well as water (Reaction 3) take place as the cathodic reactions.[28,29] Regarding the iron sulfide electrode, the nature of the reactions have not been identified yet, but we will review the potential reactions that were proposed in literature in the following section.

$$Fe_{(s)} \rightleftharpoons Fe^{2+}{}_{(aq)} + 2e^{-} \quad [1]$$

$$2H^{+}{}_{(aq)} + 2e^{-} \rightleftharpoons H_{2(g)} \quad [2]$$

$$2H_2O_{\ (l)} + 2e^{-} \rightleftharpoons H_{2(g)} + 2OH^{-}{}_{(aq)} \quad [3]$$

Prior to presenting the results of galvanic coupling measurements, it is worth mentioning that we have used the graphical calculation of the galvanic current from polarization measurements as an additional method to support our ZRA measurements and to gain better mechanistic understanding of the results observed in different conditions. However, it should be considered that ZRA measurement is the most accurate technique for the measurement of a galvanic coupling experiment in which the galvanic current and potential are directly obtained. The polarization curves can be also used for the estimation of galvanic corrosion as has been shown in numerous studies.[30–35] Hence, it could be valuable to briefly describe how galvanic current can be quantified using this method.

Figure 3b qualitatively represents the polarization curves for a general galvanic coupling measurement and the method for determining the associated galvanic current and potential. In a general case, the galvanic or coupled potential, in other words the potential at which both electrodes stabilize, is found as the intersection of total anodic currents and total cathodic currents. As a result, Eq. 4 applies at coupled potential in which $I^{A}_{c,coupled}$ and $I^{A}_{a,coupled}$ are the cathodic and anodic current of anode, while $I^{C}_{c,coupled}$ and $I^{C}_{a,coupled}$ indicate the cathodic and anodic current of cathode. It should be considered that Eq. 4 is only valid when the ohmic solution resistance is negligible.

$$I^{A}_{c,coupled} + I^{C}_{c,coupled} = I^{A}_{a,coupled} + I^{C}_{a,coupled} \quad [4]$$

Since anode, or the less noble metal, is corroded, the galvanic current can be defined as the corrosion current of anode due to the external cathode. Noting that the anodic reaction at the surface of anode plays as the source of electrons for the cathodic reaction occurs at the surface of anode as well as the one occurs at the surface of external cathode. That being the case, the galvanic current, $I_{galvanic}$, can be determined using Eq. 5.[36,37]

$$I_{galvanic} = I^{A}_{a,coupled} - I^{A}_{c,coupled} \quad [5]$$

As mentioned earlier, Eq. 5 represents the galvanic current for any general case of galvanic coupling. However, in many practical situations, the corrosion current due to the cathodic reaction at the surface of anode is much smaller than that due to the external cathode, and therefore it can be neglected. In this case, the galvanic current is simply assumed as the intersection of cathode's cathodic curve and anode's anodic curve which can also be represented as Eq. 6. We will discuss later that this assumption is valid for all the conditions studied here except one case.

$$I_{galvanic} = I^{A}_{a,coupled} = I^{C}_{c,coupled} \quad [6]$$

Effect of iron sulfide type on galvanic corrosion between mild steel and iron sulfides.—As already mentioned, pyrite and pyrrhotite were selected as iron sulfide types to be investigated. This section looks into how these iron sulfides behave differently when coupled to X65 steel electrode and we will discuss the probable origins of the difference between the electrochemical responses of pyrite and pyrrhotite.

Figure 4 displays the cathodic and anodic polarization measurements for X65 steel and iron sulfides at 1 wt.% NaCl and cathode to anode surface area ratio of 1. It is worth mentioning that the axis ranges of figures (a) and (b) are similar so that the results could be visually comparable. It can be clearly seen that the cathodic current of pyrrhotite is much greater than pyrite in the same experimental condition, which would lead to a higher rate of galvanic current. For each case, we calculated the total cathodic current (black dashed lines) by adding the cathodic current of mild steel to that of pyrrhotite or pyrite. The cathodic current of mild steel was simply

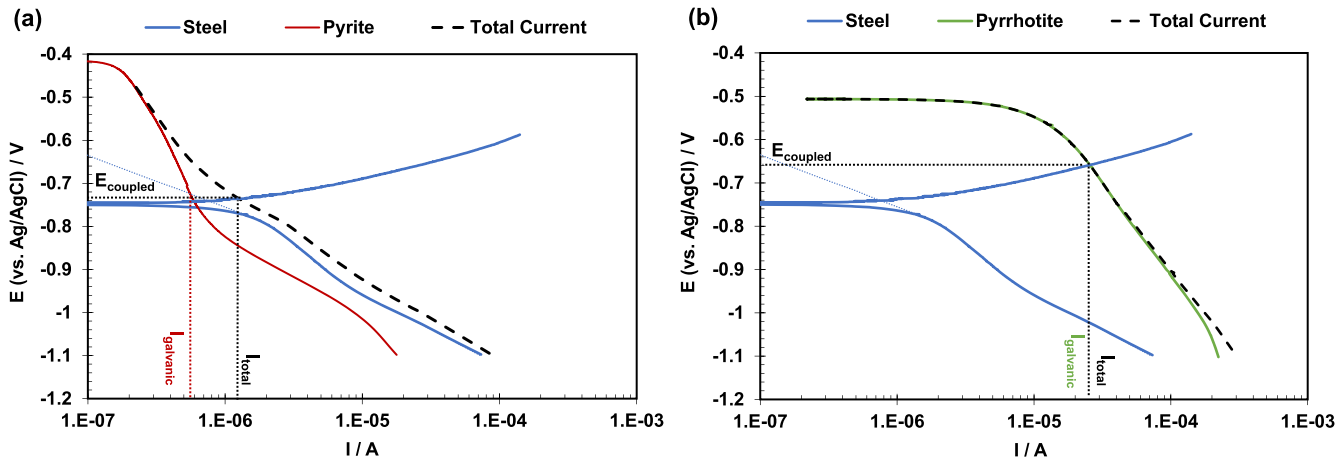

Figure 4. Potentiodynamic polarizations curves and the associated galvanic coupling calculations for (a) mild steel-pyrite, and (b) mild steel-pyrrhotite couples at 30 °C, 1 wt.% NaCl, pH 5, and cathode:anode surface area ratio of 1:1. ($E_{coupled}$ is the galvanic potential, $I_{galvanic}$ is the galvanic current, and I_{total} is the total corrosion current. The blue dotted line is the calculated cathodic current on steel, and the black dashed lines are the calculated total cathodic currents.).

calculated as an extrapolation of measured cathodic current into the more positive potential region using 0.12 V·decade^{-1} Tafel slope associated with the H^+ reduction (Reaction 2) occurring in this region.[28,38–40] Also noting that the anodic current related to the iron sulfides has been disregarded since their values are much lower than anodic current of mild steel in the potential range of interest. Also, it should be considered that cathodic current of mild steel is slightly higher than that of pyrite, and thus it should not be ignored. This fact implies that the total corrosion current, I_{total}, is not equal to the galvanic corrosion current. Therefore, Eq. 5 should be applied in this scenario to calculate the galvanic current. In addition, it can be estimated graphically as simply the cathodic current of pyrite at the coupled potential.

On the other hand, the total cathodic current of pyrrhotite is approximately equivalent to the cathodic current of pyrrhotite as its current is up to two orders of magnitude higher than the cathodic current of mild steel. Accordingly, by neglecting the cathodic current on steel, the intersection of cathodic current of pyrrhotite with anodic current of steel can be estimated as galvanic current and coupled potential. As we saw, this common simplification was not true in one case of our study, i.e., mild steel-pyrite couple. For each iron sulfide, we graphically estimated the galvanic current and coupled potential. As illustrated in Fig. 4, the coupled potentials are −0.735 and −0.66 V vs Ag/AgCl, and the galvanic currents are around 5.3×10^{-7} and 2.4×10^{-5} A for pyrite and pyrrhotite, respectively.

As observed in Fig. 4, pyrrhotite shows a very different cathodic behavior compared with pyrite which resulted in around two orders of magnitude higher galvanic current. The origin of this distinction emerges from their different physicochemical characteristics which cause different electrochemical reactions occurring on the surface of iron sulfides. Although the electrochemical characteristic of iron sulfides is very complex and thus it is beyond the scope of this paper, we concisely describe the probable electrochemical reactions to assist the interpretation of the results obtained here.

Pyrite with the chemical formulae of FeS_2 is stoichiometric iron sulfide and the most thermodynamically stable phase of the iron sulfides.[6] Pyrite was reported as the final phase of iron sulfide transformation and thus as the long-term corrosion products of steel in H_2S environments.[4,5] In contrast, pyrrhotite is defined a group of non-stoichiometric iron sulfides formulated as $Fe_{1-x}S$.[6] Therefore, it is expected that pyrite has lower reactivity compared to pyrrhotite due to its high stability.

Very few studies focused on the cathodic reactions occurring on the iron sulfides specifically in acidic solutions. The only systematic research, done by Navabzadeh et al.,[41] investigated the cathodic behavior of X65 steel, pyrite, and pyrrhotite in various acidic solutions at different bulk solution pH using a rotating disk electrode apparatus. At low pH values (pH ⩽ 4), and also at low overpotentials where hydrogen evolution reactions due to H^+ ion reduction as well as water reduction are dominant, pyrite and pyrrhotite showed similar cathodic current as X65 steel. But the cathodic current of pyrrhotite was approximately one order of magnitude higher than pyrite at pH 5, which agrees with the results obtained here indicating the higher electrochemical activity of pyrrhotite.[41] Navabzadeh et al. further analyzed these reactions by comparing the cathodic current of mineralogical pyrrhotite in various experimental conditions and showed that the cathodic reaction occurring on pyrrhotite at more positive overpotential is the conversion of pyrrhotite to troilite, similar to what has been proposed by Mikhlin.[42] These findings suggest that where hydrogen evolution is not dominant (i.e., high overpotential, pH 5), additional cathodic reactions could occur on the surface of iron sulfides which leads to the higher cathodic current produced by pyrrhotite.

Previous studies suggested various cathodic reactions taking place on pyrite surface apart from hydrogen evolution reaction. The main proposed cathodic reaction could be attributed to the reduction of pyrite in acidic solutions according to Reaction 7,[43,44] and the reduction of polysulfide (Reaction 8) as an impurity formed during the geological formation of pyrite.[45,46]

$$FeS_{2(s)} + 2H^+_{(aq)} + 2e^- \rightleftharpoons FeS_{(s)} + H_2S_{(g)} \quad [7]$$

$$S^{2-}_{n(s)} + 2(n-1)e^- \rightarrow nS^{2-}{}_{(s)} \quad [8]$$

The investigation of cathodic reactions on the surface of pyrrhotite was examined in more detail in several previous studies. In earlier papers, Hamilton et al.[47] believed that the reduction of iron oxide could occur on pyrrhotite similar to what was observed on pyrite. However, Nicol et al.[48] suggested that non-stoichiometric pyrrhotite could be reduced to stoichiometric iron sulfide FeS. The reduction of pyrrhotite can occur in two different ways: solid-state reduction of pyrrhotite to troilite,[49] and reductive dissolution of pyrrhotite,[42,48] as represented by Reaction 9 and Reaction 10, respectively. The reduction of polysulfides (Reaction 7) was also proposed for pyrrhotite.[42,45,50]

$$Fe_{(1-x)}S_{(s)} + xH^+_{(aq)} + 2xe^- \rightarrow (1-x)FeS_{(s)} + xHS^-_{(aq)} \quad [9]$$

$$Fe_{(1-x)}S_{(s)} + H^+_{(aq)} + 2xe^- \rightarrow (1-x)Fe^{2+}_{(aq)} + HS^-_{(aq)} \quad [10]$$

Although these studies could not exactly identify the nature of the electrochemical reactions, the higher cathodic current of pyrrhotite

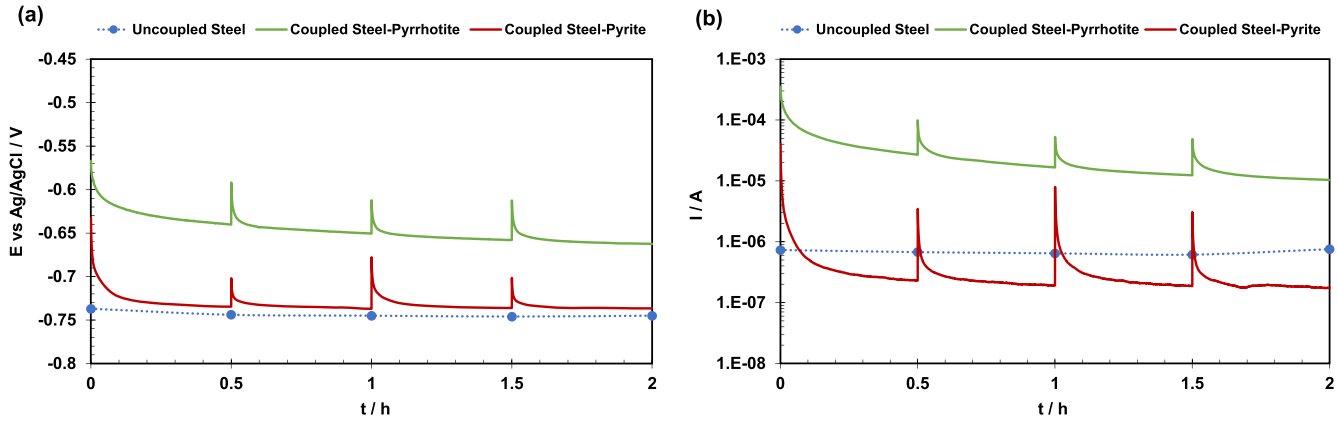

Figure 5. (a) Galvanic potential, and (b) galvanic current of steel when coupled to pyrite and pyrrhotite at 30 °C, 1 wt.% NaCl, pH 5, cathode/anode ratio = 1. (The blue dotted lines represent the open circuit potential and corrosion current of uncoupled steel measured every 0.5 h.).

can be associated with its lower stability as well as its higher tendency to be reduced to different compounds in various corrosive environments.[45,51] It is worthful to discuss that in addition to the reactivity of iron sulfides, their electronic properties might also play a role in their cathodic behaviors. Pyrite has been reported to show different semiconductive behavior including p-type, n-type, and sometimes alternating n-p type semiconductors.[52,53] According to Abraitis et al.,[52] the conductivity of pyrite ranges from 0.02 to 562 $(\Omega{\cdot}cm)^{-1}$ with the mean value being 47.64 $(\Omega{\cdot}cm)^{-1}$. However, the conductivity significantly depends on the type of semiconductor with n-type being more conductive than the p-type (mean conductivity values for n-type and p-type samples are 65.08 and 0.53 $(\Omega{\cdot}cm)^{-1}$, respectively).[52] Pascual et al.[54] observed that the transition from pyrrhotite to pyrite is accompanied by the transition from n-type to p-type behavior, and thus by the decrease in conductivity. In a review paper by Pearce et al.,[55] the electrical resistivity of pyrrhotite samples were found to be much lower than that of pyrite samples, and in some cases, pyrrhotite samples even showed metallic behavior.[55,56] Overall, these studies suggest that the higher conductivity of pyrrhotite might also contribute to the higher cathodic current observed here.

According to the experimental procedure described earlier, we measured the coupled potential and the galvanic current for steel-pyrite and steel-pyrrhotite couples using ZRA method, and the results are plotted in Figs. 5a and 5b, respectively. The blue dotted line represents the corrosion potential (Fig. 5a) and corrosion current (Fig. 5b) of uncoupled steel which was measured every 30 min as shown by points. Although these data represent the current and potential of uncoupled steel only during mild steel-pyrite coupling measurement, the values of current and potential during mild steel-pyrrhotite couple measurement were only slightly different. More importantly, we did not observe the change of potential and current for uncoupled steel during any 2-hour galvanic coupling measurements. This observation indicates that the mild steel surface have not undergone any major changes during galvanic coupling. It is worth noting that the spikes observed every 30 min in the data were due to the disconnection and reconnection of the electrodes at these times, used for measuring the potential and corrosion current of uncoupled steel. When reconnecting the electrodes, the spikes appeared due to the sudden polarization of the mild steel at the beginning of the coupling followed by the quick stabilization of the measurement. It should also be mentioned that the results shown in these graphs are for one of the replicates in each condition. Since the results were highly reproducible, and also for the sake of more clarity in the graphs, only one replication was shown here. The reproducibility of the results for two replications will be shown using error bars for the corrosion rate data. As Fig. 5 shows, the increase in mild steel potential when coupled to pyrite was less than 10 mV, while it was around 100 mV when coupled to pyrrhotite, with its ability to significantly polarize steel. The coupled potential found from galvanic measurements (−0.733 V for pyrite and −0.646 V for pyrrhotite) match very well with our predictions from measured polarization curves.

Furthermore, the galvanic current of steel-pyrrhotite couple was notably higher than the galvanic current of steel-pyrite couple which was less than the intrinsic corrosion current of uncoupled steel. We can derive the same conclusion obtained from polarization data that the higher cathodic current on the pyrrhotite electrode could originate from the higher reducibility of pyrrhotite as discussed earlier. The values of galvanic current measured during galvanic coupling experiments (3.90×10^{-7} A for pyrite and 2.56×10^{-5} A for pyrrhotite) are in line with the values derived from polarization measurements considering that the values calculated for galvanic current measurements are the average values obtained during the two-hour long experiments (also the average value of two repeats). On that account, the results show the agreement between the polarization and the galvanic coupling measurements.

Lastly, the corrosion rates of uncoupled steel, coupled steel-pyrite, and coupled steel-pyrrhotite were determined for the above-mentioned experiments and are presented in Fig. 6. The corrosion rates were calculated using Eq. 11 in which M_{Fe} is molecular weight of iron 55.845, ρ_{Fe} is density of iron equal to 7874 $Kg{\cdot}m^{-3}$, n is equivalent number of 2 for iron, and F is faraday constant 96485 $s{\cdot}A{\cdot}mol^{-1}$.

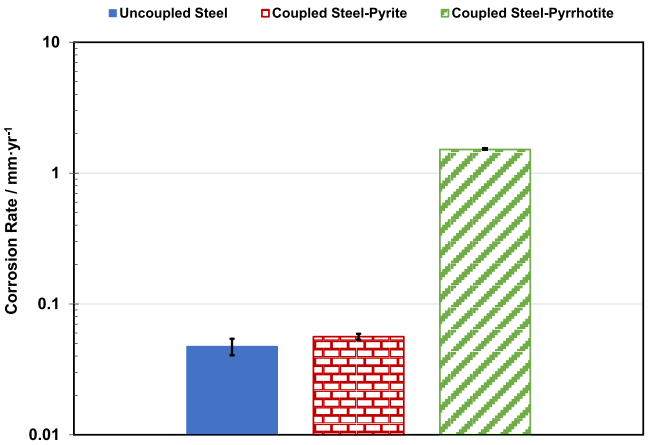

Figure 6. Calculated corrosion rates of uncoupled X65 mild steel and coupled mild steel-iron sulfides at 30 °C, 1 wt.% NaCl, pH 5, cathode:anode surface area ratio of 1:1. The reported values are the average of two replications with error bars representing the range of replications.

$$Corrosion\ Rate(CR) = \frac{i_{corr} M_{Fe}}{\rho_{Fe} nF} \quad [11]$$

Note that i_{corr} is the total corrosion current density of steel which includes the corrosion of steel due to the external connection to the iron sulfide cathode as well as the cathodic reaction occurring simultaneously on the mild steel surface. The most accurate way to evaluate the total corrosion current is direct graphical estimation of I_{total} from polarization measurements. However, in cases when Eq. 6 applies (i.e., all cases except coupled steel-pyrite with cathode:anode ratio of 1:1), the galvanic current value found from galvanic coupling measurements can be used instead. As was seen and will be shown later in a more complete format, the experimental results from both methods agree very well, but for the sake of consistency, all the corrosion rate calculations were based on the current values from galvanic measurements. To conclude, Fig. 6 reveals that the corrosion rate of steel does not significantly increase due to the coupling to pyrite, while it increases by about an order of magnitude when coupled to pyrrhotite.

Effect of cathode to anode surface area ratio on galvanic corrosion between mild steel and iron sulfides.—The importance of cathode to anode surface area ratio during galvanic corrosion between two dissimilar metals has been subjected to many research papers[33,57,58] because in most situations, the surface area of cathode differs from that of anode. In fact, the major issue is observed when the cathode's surface area is much larger than the anode which results in severe localized corrosion of anode. It has been previously shown that the galvanic current of various materials including carbon steel, when coupled to a more noble metal, is significantly amplified by increasing the cathode to anode surface area ratio.[33,57–60] In corrosion of mild steel in H_2S environments, in some cases, the high porosity of the iron sulfide corrosion product layer formed during the corrosion process increases the available cathodic surface area compared with the surface of mild steel. We investigated the effect of larger cathode to anode surface area ratio by varying the surface areas of mild steel and iron sulfide specimens in order to increase this ratio by approximately one and two orders of magnitude. Figure 7 compares the galvanic potentials of mild steel-pyrite and mild steel-pyrrhotite couples for different cathode to anode surface area ratios, while all other experimental parameters remained unchanged.

The coupled potential for both cases shifted to more positive value with respect to the cathode to anode surface area ratio showing that iron sulfides with the larger surface area ratio could enhance the polarization of mild steel by forcing it to stabilize at overpotential further from its intrinsic corrosion potential (~−0.740 V vs Ag/AgCl), as expected. The same observation was found when steel was galvanically coupled to different materials.[33,60] Furthermore, the coupled potentials for all cathode to anode surface area ratios for steel-pyrrhotite couples are more positive than the steel-pyrite couples suggesting the higher ability of pyrrhotite to polarizing mild steel. Galvanic current densities were also measured and compared for different cathode to anode surface area ratios as plotted in Fig. 8. It should be noted that galvanic current density was represented for these cases instead of galvanic current as mild steel sample with different surface area was used for obtaining the cathode to anode surface area ratio of 90:1.

As clearly seen in Fig. 8, the current density was increased around one and two orders of magnitude by increasing the cathode to anode surface area ratio from 1 to 8 and 90. The increase in current density was due to the increase of cathodic current associated with the larger cathodic surface area. From the viewpoint of polarization measurement, the effect of different surface areas of cathode or anode, according to Hack,[36] can be appreciated by the fact that the current is the multiplication of current density by surface area. Thus, larger surface area of cathode shifts its polarization curve to higher currents (or to the right in polarization plot) driving the intersection point of galvanic current to be placed at higher current values. We can also interpret these results by considering that the coupled potential, which is situated between the corrosion potential of each electrode, shifts towards the cathode (more positive potential) in case of larger cathodic surface area due to increase in its polarization driving force. Thus, mild steed is forced to be held at more positive coupled potential leading to the increase in its anodic current, and as a result its corrosion rate. It should be noted that these interpretations are valid by assuming that mild steel does not reach the passivation region of anodic current.

Similar to the previous section, corrosion rates were estimated from galvanic measurements for various cathode to anode surface area ratios, remembering that the corrosion rates shown in Fig. 9 are calculated based on the total corrosion current density as discussed earlier. Noticing the logarithmic scale, the corrosion rate of both steel-pyrite and steel-pyrrhotite couples are nearly one and two orders of magnitudes higher for cathode to anode area ratios of 8:1 and 90:1, respectively, when compared to the corrosion rate of 1:1 cathode to anode surface area ratio. The intensification of cathodic current of larger cathode, as we explained above, is the cause of increase in corrosion rates. Still, the corrosion rates of mild steel-pyrrhotite couple is much higher than mild steel-pyrite couple in all cathode:anode surface area ratios thanks to its higher cathodic activity.

Effect of aqueous solution conductivity (NaCl concentration) on galvanic corrosion between mild steel and iron sulfides.—The influence of changing aqueous solution conductivity via changing NaCl concentration was another experimental factor that was investigated. In theory, the degree of conductivity could determine

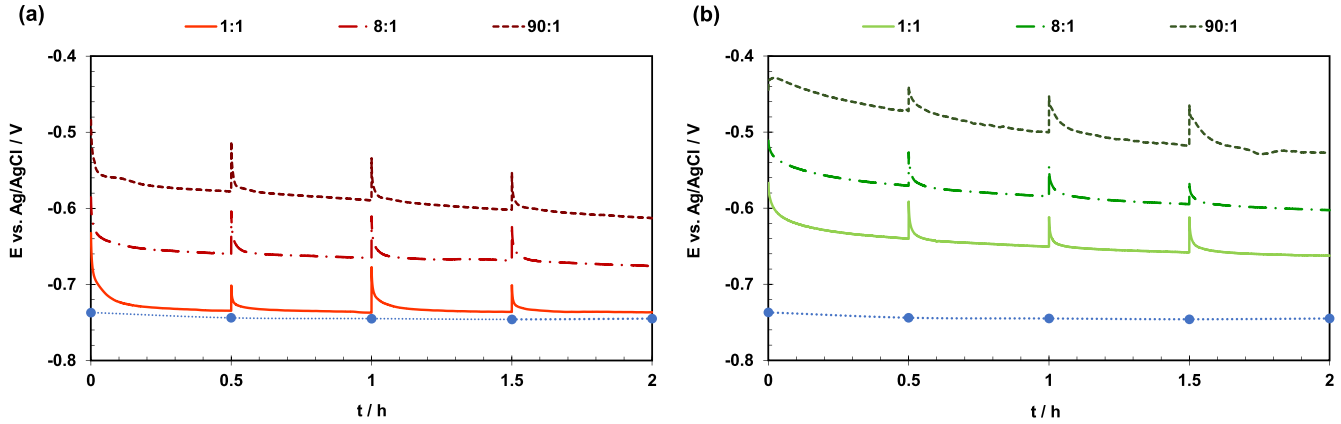

Figure 7. The effect of cathode to anode surface area ratio on the galvanic potential of mild steel when coupled to (a) pyrite, and (b) pyrrhotite at 30 °C, 1 wt.% NaCl, and pH 5. (The blue dotted line shows the open circuit potential of uncoupled mild steel measured every 0.5 h.).

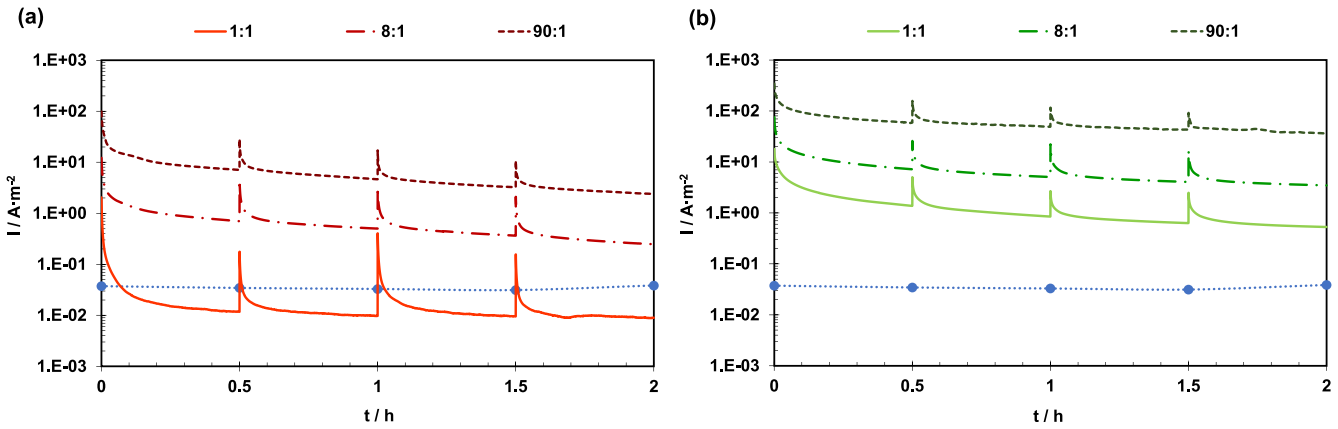

Figure 8. The effect of cathode to anode surface area ratio on the galvanic current of mild steel when coupled to (a) pyrite, and (b) pyrrhotite at 30 °C, 1 wt.% NaCl, and pH 5. (The blue dotted line shows corrosion current density of uncoupled mild steel measured every 0.5 h.).

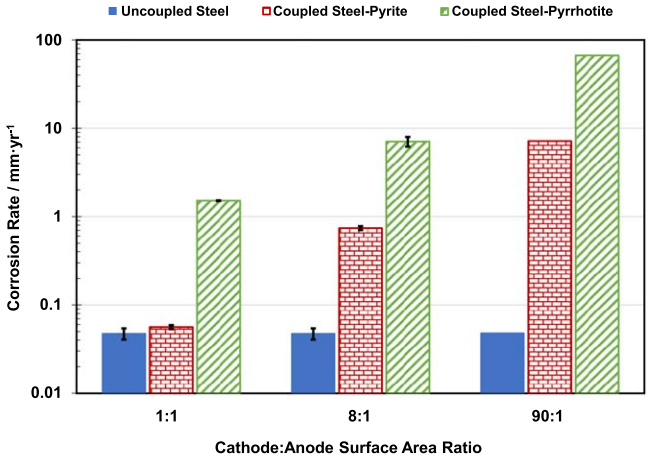

Figure 9. The effect of cathode to anode surface area ratio on corrosion rates of uncoupled X65 mild steel and coupled mild steel-iron sulfides at 30 °C, 1 wt.% NaCl, pH 5. For the data with error bars, the reported values are the average of two replications with error bars representing the range of replications.

the solution's capacity to transfer ions. Improving the conductivity of solutions in a galvanic couple facilitates the transfer of ions between anode and cathode, thereby enhancing the reactions occurring on both electrodes. Thus, we expect that increasing NaCl concentration could lead to a higher galvanic current. The NaCl concentration was changed from 0.1 to 10 wt.% (from 0.017 to 1.71 M) in this study. Our effort was to vary the NaCl concentration by one and two orders of magnitude, such that the effect of this factor would be clearly noticeable. The conductivity of the solutions, based on the chemistry handbooks,[61] are 0.15, 1.6, and 12.6 $S \cdot m^{-1}$ for 0.1, 1, and 10 wt.% NaCl, respectively, showing that the conductivity is also increased by approximately the same order of magnitude. The specific design of the electrochemical setup with a small distance (2 cm) between cathode and anode effectively minimized the ohmic resistance between the electrodes. The solution resistance between the reference electrode (placed between the anode and cathode) and mild steel were around 350, 40 and 7 ohms for 0.1, 1, and 10 wt.% NaCl, respectively. Considering the low galvanic current values, the contribution of iR drop due to the solution resistance was negligible, specifically for the cathode to anode surface area ratios of 1:1 and 8:1 that were investigated in this section.

Figure 10 compares the galvanic current for both steel-pyrite and steel-pyrrhotite couples for solutions with various NaCl concentrations for cathode to anode surface area ratio of 1:1. The corrosion current of uncoupled steel is shown similar to previous figures, only for 1 wt.% NaCl solution. As we will argue later, the corrosion current of uncoupled steel itself is also changing with NaCl concentration; however, this change is minimal compared to the galvanic current change for galvanic couples.

For mild steel-pyrrhotite couple, the galvanic current increased from 1.07×10^{-5} A to 2.56×10^{-5} A when NaCl concentration changed from 0.1 wt.% to 1 wt.%. However, further increase of NaCl concentration to 10 wt.% showed only a minor effect on galvanic current. On the other hand, the change of NaCl concentration did not clearly impact the galvanic current of mild steel-pyrite couple. As it is seen, the results did not meet the expectation that higher conductivity generally enhances galvanic corrosion. Since the effect of NaCl concentration was observed for mild steel-pyrrhotite couple, we can initially select this case to analyze the obtained results. In general, electrolytes with high conductivity produce better current and potential distribution across the surface of anode leading to higher galvanic corrosion.[33,62] Furthermore, higher conductivity accelerates the transport of the ionic electrical current in the solution which results in higher rates of electrochemical reactions at the metal surface. As a consequence, it is feasible to observe higher galvanic current when NaCl concentration is increased from 0.1 to 1 wt.% in mild steel-pyrrhotite couple. However, such an increase was not observed when NaCl concentration changed from 1 wt.% to 10 wt.%. This peculiarity can be clarified by investigating the effect of NaCl concentration on electrochemical reactions of mild steel.

Salt concentration was extensively shown to influence the electrochemical reaction rate, specifically iron dissolution reaction.[39,63,64] Madani Sani investigated the effect of a wide range of NaCl concentration (from 0 to 20 wt.% NaCl) on corrosion rates as well as electrochemical reactions of mild steel in weak acid solutions (i.e., aqueous CO_2 solution) and found that ion concentration changes the electrochemical reaction rate of both cathodic and anodic reactions on the surface of steel due to the change of exchange current density of these reactions. In particular, the rate of iron dissolution reaction increased by the increase of NaCl concentration up to 3 wt.% and then dramatically decreased at higher NaCl concentration.[39] Similar trend for influence of NaCl on iron dissolution reaction was observed in other studies, for instance, papers by Fang et al. and Liu et al.[63,65] Iron dissolution reaction occurs through adsorption of OH^- ion via either well-known Bockris mechanism or catalytic mechanism proposed by Heusler.[28,66] It was suggested that Cl^- ion can also adsorb to the surface of iron and catalytically enhance the iron dissolution reaction through a similar pathway parallel to OH^- adsorption.[63,67,68] However, it was shown that the effect of OH^- on iron dissolution rate is stronger than Cl^- ions.[49] Therefore, very high concentration of Cl^- ion could significantly retard the adsorption of OH^- ion, decrease its surface coverage on iron surface, and consequently reduce the

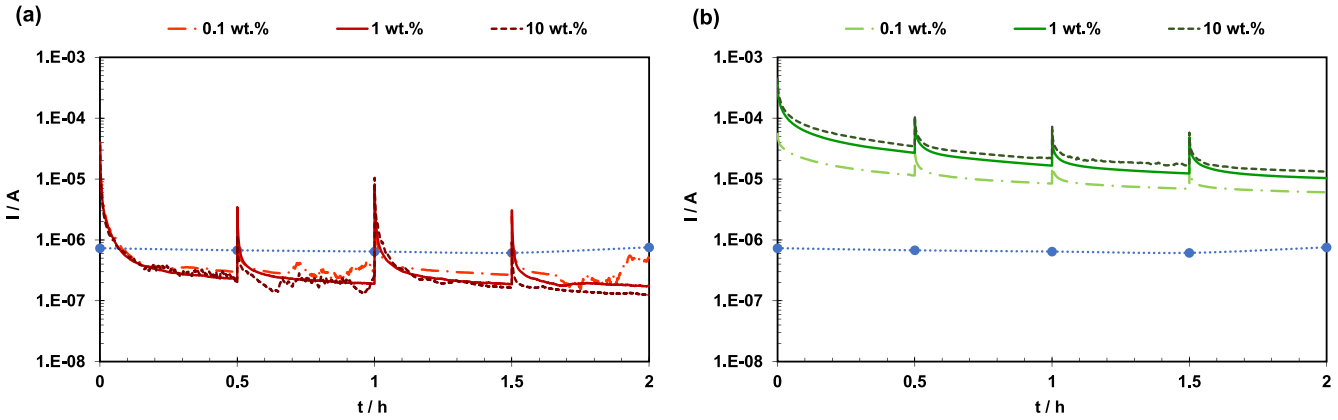

Figure 10. The effect of NaCl concentrations on the galvanic current of mild steel when coupled to (a) pyrite, and (b) pyrrhotite at 30 °C, pH 5, and cathode: anode surface area ratio of 1:1. (The blue dotted line shows corrosion current density of uncoupled mild steel measured every 0.5 h.).

electrochemical reaction rate.[69] In addition, it was suggested that the retardation of iron dissolution rate could stem from the retardation of water activity at high NaCl concentrations which was demonstrated previously by Madani Sani et al.[39,70]

For further exploration, we have measured the cathodic and anodic reaction of mild steel in all three NaCl concentrations (Fig. S3). We should note here that we did not observe noticeable change for the electrochemical reactions of iron sulfides in various NaCl concentrations. The polarization results of mild steel (Fig. S3) were in line with the previous studies showing that the rate of electrochemical reactions are slightly retarded when NaCl concentration increased to 10 wt.% NaCl. The same observation was shown in a recent paper by Standish et al. in which they measured the influence of chloride concentration on the galvanic coupling between carbon steel and copper.[33] The galvanic current increased by increasing NaCl concentration from 0.001 M up to 0.1 M, then decreased by further increase of NaCl concentration to 3.0 M. The cause was revealed by potentiodynamic polarization curves which showed the retardation of both carbon steel anodic reaction rate as well as copper cathodic reaction rate.[33] In our case, the slight retardation of electrochemical activity in 10 wt.% NaCl might be compromised by slight enhancement in ion transport and current distribution in this solution, which result in similar galvanic current for 1 and 10 wt.% NaCl.

With regard to mild steel-pyrite couple, the indistinguishable change of galvanic current in various NaCl concentrations could also be explained through the effect of NaCl concentration on electrochemical reactions. For the cathode to anode surface area ratio of 1:1, the cathodic currents of both mild steel and pyrite contribute to the total cathodic current (as seen in Fig. 4a) and thus to the final coupled potential. Therefore, the retardation of cathodic current of mild steel in 0.1 wt.% could only slightly decrease the total cathodic current. Also, considering the small retardation of anodic current of mild steel at the potential region just above OCP (Fig. S3), the coupled potential of 0.1 wt.% NaCl would be minimally higher than that of 1 wt.% NaCl. Since galvanic current is the cathodic current of pyrite at coupled potential, the change of NaCl concentration does not cause a noticeable change in the galvanic current values. For further clarification, we examined the influence of NaCl concentration on the galvanic current for cathode to anode surface area ratio of 8:1 (Fig. S4). In this condition, the cathodic current of mild steel is negligible compared with that of pyrite and the retardation of anodic current is more notable at higher overpotential region. Although we observed that the galvanic current slightly increased by the increase of 0.1 to 1 wt.% NaCl, the results suggest that the solution conductivity is not an important factor in galvanic corrosion of mild steel-pyrite couple in the specific design of our study.

Lastly, corrosion rates were calculated for various NaCl concentrations for cathode to anode surface area ratios of 1:1 and 8:1, as demonstrated in Fig. 11. The increase of NaCl concentration from 0.1 wt.% to 1 wt.% resulted in a notable increase in corrosion rate for mild steel-pyrrhotite couple, however, the change of corrosion rate was not significant when NaCl concentration increased to 10 wt.%. For mild steel-pyrite couple, the corrosion rate was not affected by NaCl concentration for cathode to anode surface area ratio of 1:1 since very low current was produced at this condition and low

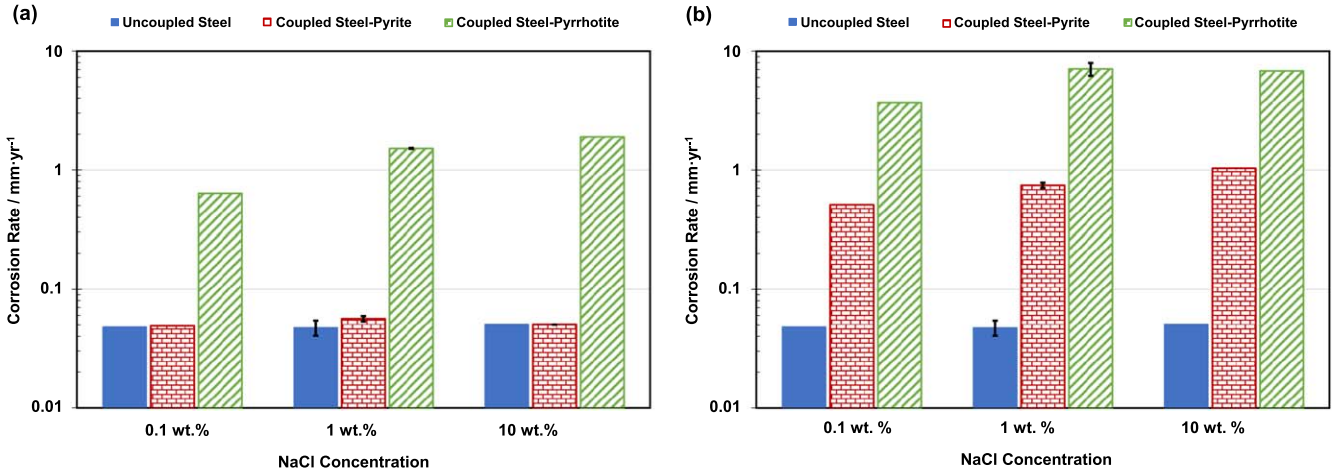

Figure 11. The effect of NaCl concentration on corrosion rates of uncoupled X65 mild steel and coupled mild steel-iron sulfides at 30 °C, pH 5, and cathode: anode surface area ratios of (a)1:1, and (b) 8:1. For the data with error bars, the reported values are the average of two replications with error bars representing the range of replications.

Table II. Summary of galvanic corrosion measurements at various conditions.

Galvanic couple	NaCl conc. (wt.%)	Cathode:Anode surface area ratio	Galvanic current density ($A \cdot m^{-2}$)	Coupled potential (mV vs Ag/AgCl)	Total current density ($A \cdot m^{-2}$)	Total galvanic corrosion rate ($mm \cdot yr^{-1}$)
Mild steel (uncoupled)	0.1	—	—	—	0.041	0.048
	1	—	—	—	0.041	0.047
	10	—	—	—	0.043	0.050
Mild steel-pyrite	0.1	1	0.022	−0.719	0.042	0.049
		8	0.438	−0.656	0.438	0.508
	1	1	0.020	−0.733	0.048	0.056
		8	0.640	−0.662	0.641	0.742
		90	6.161	−0.588	6.161	7.150
	10	1	0.017	−0.728	0.043	0.050
		8	0.890	−0.645	0.890	1.033
Mild steel-Pyrrhotite	0.1	1	0.545	−0.630	0.545	0.633
		8	3.178	−0.514	3.178	3.688
	1	1	1.306	−0.646	1.306	1.519
		8	6.107	−0.580	6.107	7.087
		90	57.62	−0.491	57.62	66.88
	10	1	1.634	−0.630	1.634	1.896
		8	5.868	−0.580	5.868	6.811

conductivity of 0.1 wt.% NaCl was capable of transporting this current. However, a marginally higher corrosion rate for 1 wt.% NaCl compared with 0.1 wt.% NaCl can be observed when cathode to anode surface area ratio was 8:1. It is worth comparing that the impact of NaCl concentration is not similar to the impact of cathode to anode surface area ratio, in the sense that increase of NaCl concentration by one and two orders of magnitude does not increase the galvanic corrosion by the same orders.

A summary of the galvanic corrosion results obtained from ZRA method at various experimental conditions is provided in Table II. We should remind that, for the conditions with two replications (shown with error bar in corrosion rate figures), the reported values are the average of those replications. Furthermore, we discussed and compared the corrosion rates data obtained from ZRA with those from polarization measurements in supplementary materials (Figs. S5–S8). The results showed very good agreement between the corrosion rate data found from ZRA and polarization methods.

As a final consideration, we can report that the effect of pH was also examined since it could play an important role in the galvanic corrosion of mild steel in some cases with more acidic H_2S environments. However, this factor was not included in the main text of this paper as the influence of pH on electrochemical reactions of both iron sulfides and mild steel is very complex and is not fully well-known. Here, it suffices to say that the measurements at pH 4 increased the galvanic corrosion rate of mild steel-pyrite couple but had no influence on the mild steel-pyrrhotite couple (Figs. S9–S10). We provided a brief discussion on the effect of pH in supplementary materials.

Conclusions

In the present study, we investigated the impact of three experimental factors on the galvanic corrosion between X65 carbon steel and iron sulfides, namely: the type of iron sulfide, the cathode to anode surface area ratio, and the concentration of NaCl. This was done by monitoring galvanic current and coupled potential in zero-resistance ammeter (ZRA) experiments as well as by analyzing the polarization behavior of electrodes. Our main findings are:

- In the studied experimental conditions i.e., pH 5, at 30 °C, the galvanic behavior of mild steel-pyrite distinctly differed from that of mild steel-pyrrhotite couple. For cathode to anode surface area ratio of 1:1, coupling of mild steel to pyrite did not significantly change the corrosion rate of mild steel while its coupling to pyrrhotite increased the corrosion rate of mild steel by around an order of magnitude.
- This difference was related to the different electrochemical behavior of pyrite and pyrrhotite by analyzing their polarization response. In addition, the experimental data obtained from galvanic corrosion measurements using ZRA method were in a very good agreement with the values of galvanic current and couple potential calculated through polarization graphs.
- When cathode to anode surface area ratio was increased to 8:1 and 90:1, the galvanic corrosion rates of both mild steel-pyrite and mild steel-pyrrhotite couples were increased by approximately the same order of magnitude.
- Finally, increasing the conductivity of the aqueous solution by increasing the NaCl concentration from 0.1 wt.% to 1 wt.% slightly increased the galvanic corrosion of mild steel-pyrrhotite couple in all tested conditions and the galvanic corrosion of mild steel-pyrite couple only for 8:1 surface area ratio. However, very high salt concentrations i.e., 10 wt.% NaCl did not increase the galvanic corrosion, even if the solution conductivity was much higher.

Acknowledgments

The author would like to thank the following companies for their financial support: Ansys, Baker Hughes, BP, Chevron Energy Technologies, Clariant Corporation, CNOOC, ConocoPhillips, M-I SWACO (Schlumberger), Multi-Chem (Halliburton), Occidental Oil Company, Pertamina, Saudi Aramco, Shell Global Solutions, SINOPEC (China Petroleum), and TotalEnergies.

ORCID

Payman Sharifi Abdar https://orcid.org/0000-0003-4072-8293

References

1. M. B. Kermani and D. Harrop, *SPE Production & Facilities*, **11**, 186 (1996).
2. J. Kvarekval, *CORROSION*, Salt Lake City, Utah (NACE International) 1537 (2012).
3. J. Kvarekval and G. Svenningsen, *CORROSION*, Dallas, Texas (NACE International) 5720 (2015).
4. J. Ning, Y. Zheng, B. Brown, D. Young, and S. Nešić, *Corrosion*, **73**, 155 (2016).
5. J. Ning, Y. Zheng, D. Young, B. Brown, and S. Nešić, *Corrosion*, **70**, 375 (2013).

6. D. Rickard and G. W. Luther, *Chem. Rev.*, **107**, 514 (2007).
7. D. Rickard and J. W. Morse, *Mar. Chem.*, **97**, 141 (2005).
8. S. N. Esmaeely and S. Nešić, *Corrosion*, **75**, 938 (2019).
9. S. Gao et al., *Corrosion*, **73**, 915 (2017).
10. S. Gao et al., *Corrosion*, **73**, 1188 (2017).
11. F. Pessu, R. Barker, and A. Neville, *Corrosion*, **73**, 1168 (2017).
12. F. Pessu, Y. Hua, R. Barker, and A. Neville, *Corrosion*, **74**, 886 (2018).
13. F. H. Meyer, O. L. Riggs, R. L. McGlasson, and J. D. Sudbury, *Corrosion*, **14**, 69 (1958).
14. J. S. Smith and J. D. A. Miller, *Br. Corros. J.*, **10**, 136 (1975).
15. J. Ning, Y. Zheng, B. Brown, D. Young, and S. Nesic, *CORROSION*, Phoenix, Arizona (NACE International) 10905 (2018).
16. M. Tjelta and J. Kvarekval, *CORROSION*, Vancouver, British Columbia (NACE International) 7478 (2016).
17. O. Yepez, N. Obeyesekere, and J. Wylde, *CORROSION*, Vancouver, British Columbia (NACE International) 7795 (2016).
18. P. S. Abdar, B. Brown, and S. Nesic, *AMPP*, San Antonio, Texas (AMPP) 17827 (2022).
19. S. Navabzadeh Esmaeely, *thesis*, Ohio University (2018).
20. M. Tjelta and J. Kvarekval, *CORROSION*, New Orleans, Louisian (NACE International) 9319 (2017).
21. J. Kvarekvål and G. Svenningsen, *CORROSION*, Vancouver, British Columbia (NACE International) 7313 (2016).
22. J. Ning, *thesis*, Ohio University (2016).
23. S. Uchiyama et al., *ACS Omega*, **6**, 31358 (2021).
24. F. W. Herbert, A. Krishnamoorthy, L. Rands, K. J. V. Vliet, and B. Yildiz, *Phys. Chem. Chem. Phys.*, **17**, 11036 (2015).
25. R. G. Arnold, *The Canadian Mineralogist*, **9**, 31 (1967).
26. Y. E. Mendili, A. Abdelouas, and J-F. Bardeau, *Phys. Chem. Chem. Phys.*, **15**, 9197 (2013).
27. Y. E. Mendili, A. Abdelouas, H. E. Hajj, and J-F. Bardeau, *RSC Adv.*, **3**, 26343 (2013).
28. P. S. Abdar, M. B. Hariri, A. Kahyarian, and S. Nesic, *Electrochim. Acta*, **382**, 138231 (2021).
29. P. Sharifi Abdar, *thesis*, Ohio University (2023).
30. K. Dong, Y. Song, F. Chang, and E-H. Han, *Electrochim. Acta*, **462**, 142662 (2023).
31. W. Yang, Z. Liu, and H. Huang, *Corros. Sci.*, **188**, 109562 (2021).
32. H. P. Hack and J. R. Scully, *Corrosion*, **42**, 79 (1986).
33. T. E. Standish, L. J. Braithwaite, D. W. Shoesmith, and J. J. Noël, *J. Electrochem. Soc.*, **166**, C3448 (2019).
34. C. Liu, J. Srinivasan, and R. G. Kelly, *J. Electrochem. Soc.*, **164**, C845 (2017).
35. S. A. Policastro, R. M. Anderson, and C. M. Hangarter, *J. Electrochem. Soc.*, **168**, 041507 (2021).
36. H. P. Hack, *Reference Module in Materials Science and Materials Engineering* (Elsevier, Amsterdam) (2016).
37. L. Yang, *Techniques for corrosion monitoring*, ed. L. Yang (Woodhead Publishing, UK) 2nd ed. (2021).
38. A. Kahyarian and S. Nesic, *Electrochim. Acta*, **297**, 676 (2019).
39. F. M. Sani, B. Brown, and S. Nesic, *J. Electrochem. Soc.*, **168**, 051501 (2021).
40. Y. Zheng, B. Brown, and S. Nešić, *Corrosion*, **70**, 351 (2013).
41. S. N. Esmaeely and S. Nesic, *J. Electrochem. Soc.*, **164**, C664 (2017).
42. Y. Mikhlin, *Phys. Chem. Chem. Phys.*, **2**, 5672 (2000).
43. B. Gong, D. Li, Z. Niu, Y. Liu, and Z. Dang, *Environ Sci Pollut Res*, **28**, 11090 (2021).
44. B. F. Giannetti, S. H. Bonilla, C. F. Zinola, and T. Rabóczkay, *Hydrometallurgy*, **60**, 41 (2001).
45. Y. Mikhlin, A. Romanchenko, and Y. Tomashevich, *Appl. Surf. Sci.*, **549**, 149261 (2021).
46. H. W. Nesbitt, G. M. Bancroft, A. R. Pratt, and M. J. Scaini, *Am. Mineral.*, **83**, 1067 (1998).
47. I. C. Hamilton and R. Woods, *J. Electroanal. Chem. Interfacial Electrochem.*, **118**, 327 (1981).
48. M. J. Nicol and P. D. Scott, *J. South Afr. Inst. Min. Metall.*, **79**, 298 (1979).
49. Y. Mikhlin et al., *Phys. Chem. Chem. Phys.*, **2**, 4393 (2000).
50. P. S. Abdar, B. Brown, and S. Nesic, *AMPP* (Denver, Colorado) (AMPP) 19428 (2023).
51. Y. Mikhlin et al., *Appl. Surf. Sci.*, **387**, 796 (2016).
52. P. K. Abraitis, R. A. D. Pattrick, and D. J. Vaughan, *Int. J. Miner. Process.*, **74**, 41 (2004).
53. R. Woods, P. E. Richardson, and F. M. Doyle, *Electrochemistry in Mineral and Metal Processing V: Proceedings of the Fourth International Symposium* (The Electrochemical Society, New Jersey, USA) (2000).
54. A. Pascual et al., *J. Phys. Chem. C*, **118**, 26440 (2014).
55. C. I. Pearce, R. A. D. Pattrick, and D. J. Vaughan, *Rev. Mineral. Geochem.*, **61**, 127 (2006).
56. D. J. Vaughan and J. R. Craig, *Mineral Chemistry of Metal Sulfides* 512 (Cambridge University Press, Cambridge) (1978).
57. D. R. Banjade, S. D. Porter, B. M. McMullan, and J. N. Harb, *J. Electrochem. Soc.*, **163**, C116 (2016).
58. J. Qiu et al., *Corros. Sci.*, **170**, 108677 (2020).
59. L. Braithwaite et al., *J. Electrochem. Soc.*, **169**, 051502 (2022).
60. C. F. Dong, K. Xiao, X. G. Li, and Y. F. Cheng, *Wear*, **270**, 39 (2010).
61. J. Rumble, *CRC Handbook of Chemistry and Physics* (CRC Press, Boca Raton, Fla) 103rd ed.1628 (2022).
62. X. G. Zhang, *Uhlig's Corrosion Handbook* (Wiley, New York) 123 (2011), https://onlinelibrary.wiley.com/doi/abs/10.1002/9780470872864.ch10.
63. H. Fang, B. Brown, and S. Nešić, *Corrosion*, **69**, 297 (2013).
64. Q. Y. Liu, L. J. Mao, and S. W. Zhou, *Corros. Sci.*, **84**, 165 (2014).
65. S. Lin, Q. Liu, and H. Li, *Chin. J. Geochem.*, **33**, 374 (2014).
66. J. O. Bockris, D. Drazic, and A. R. Despic, *Electrochim. Acta*, **4**, 325 (1961).
67. R. J. Chin and K. Nobe, *J. Electrochem. Soc.*, **119**, 1457 (1972).
68. H. C. Kuo and K. Nobe, *J. Electrochem. Soc.*, **125**, 853 (1978).
69. N. A. Darwish, F. Hilbert, W. J. Lorenz, and H. Rosswag, *Electrochim. Acta*, **18**, 421 (1973).
70. N. G. Smart, M. Gamboa-Aldeco, and J. O. Bockris, *Corros. Sci.*, **34**, 759 (1993).